Nuclear Materials and Energy 000 (2016) 1–9

Contents lists available at ScienceDirect

Nuclear Materials and Energy

journal homepage: www.elsevier.com/locate/nme

Ion orbit modelling of ELM heat loads on ITER divertor vertical targets

J.P. Gunn[a,*], S. Carpentier-Chouchana[b], R. Dejarnac[c], F. Escourbiac[d], T. Hirai[d], M. Komm[c], A. Kukushkin[e,f], S. Panayotis[d], R.A. Pitts[d]

[a] CEA, IRFM, F-13108 Saint-Paul-Lez-Durance, France
[b] EIRL S. Carpentier-Chouchana, 13650 Meyrargues, France
[c] Institute of Plasma Physics, AS CR v.v.i., Czech Republic
[d] ITER Organization, Route de Vinon-sur-Verdon, CS 90 046, 13067 St Paul Lez Durance Cedex, France
[e] NRC 'Kurchatov Institute', Moscow 123182, Russia
[f] National Research Nuclear University MEPhI, Moscow 115409, Russia

ARTICLE INFO

Article history:
Available online xxx

Keywords:
ITER
Divertor
ELM heat loads

ABSTRACT

The high heat flux areas on the vertical divertor targets in the ITER tokamak will consist of cuboid tungsten monoblocks bonded to copper cooling tubes. Three-dimensional ion orbit modelling is used to calculate the heating of tungsten monoblocks during ELMs at the inner vertical target, where the highest surface energy densities are expected. The presence of thin gaps between monoblocks results in exposed edges onto which the heat flux can be focused. ELM ions are focused by their gyromotion onto the magnetically shadowed, long toroidal edges of the monoblocks. The risk of monoblock edge melting is greater than the risk of full surface melting on the plasma-wetted zone. Alternative shaping solutions such as edge chamfering, filleting, and poloidal beveling do not show promise; the melt zone simply migrates to other locations on the monoblocks. Without ELM mitigation, there is a marginal risk of edge melting due to uncontrolled ELMs in the pre-nuclear phase of ITER operation, and an absolute certainty of it in the burning nuclear phase. To avoid edge melting altogether, the surface energy density would have to limited to less than 0.15 MJ/m^2.

1. Introduction

The ITER tokamak will begin operation with a full tungsten (W) divertor consisting of pure W monoblocks (MB) bonded to CuCrZr water-carrying cooling tubes. The predicted steady and transient thermal loads that could be delivered by the plasma to the plasma-facing components (PFC), based on physics modelling and extrapolation from current devices, and which have been used as input to the divertor design, may be found in [1] and [2]. Improved measurements of surface heat loads during ELMs are producing more refined extrapolations to ITER [3]. The predicted heat loads have until now been specified for a nominal, axisymmetric divertor surface with no gaps or surface relief caused by shaping and misalignments. The first systematic study of the detailed heat flux distribution in the gaps between MBs and the resulting thermal response due to steady inter-ELM heat loads and transient ELM loads is described in detail in [4] for the proposed divertor design (briefly described in Section 2) which consists of MBs whose top surfaces are beveled to a depth of $h_{tor} = 0.5$ mm in the toroidal direction in order to magnetically shadow poloidal leading edges. The MBs are foreseen to have sharp edges and no poloidal profiling, mainly to avoid the increased cost and manufacturing complexity that more sophisticated shaping solutions imply. In this paper, the ELM results from [4] are briefly summarized, and a number of alternative shaping solutions are studied to provide rationale for the final decision on the divertor design.

The surface heat flux factor is often employed to characterize fast transient heat loads due to edge localized modes (ELMs) since it may be referred to the melting threshold of tungsten, ~50 MJ/m^2/s$^{1/2}$ [5]. This number, deduced from high heat flux tests, gives a measure of the time it takes for the surface to reach melting temperature for a constant incident heat flux, and is confirmed by the solution of the 1D heat conduction equation on a semi-infinite domain. The heat flux factor is given by the energy flux density normal to the MB surface, divided by the square root of the heat pulse duration. An ELM heat pulse is considered to be

* Corresponding author.
E-mail address: Jamie.Gunn@cea.fr (J.P. Gunn).

http://dx.doi.org/10.1016/j.nme.2016.10.005

manageable if its heat flux factor does not exceed half the melting threshold, in order to avoid full surface melting of the MBs.

The heat flux factor is defined for a square pulse, but more realistically, the temporal evolution of ELM energy deposition is observed to increase in time to a peak value, and then decay (cf. Section 2.2.2.1 in Ref. [1]). It has been shown that the heat flux factor is not always suitable for predicting the impact of intense heat pulses onto a surface [6]. For the same total energy density deposition and pulse duration, the surface temperature rise depends on the shape of the heat pulse. Moreover, the degree of surface damage is observed to be well correlated with the maximum temperature increase rather than with the total absorbed energy density. For that reason, the calculations presented here, as in [4], will be cast into a form that makes them applicable to any heat pulse shape for a given magnetic field strength and ion temperature.

On a flat surface the temperature increase can be calculated by the 1D transient heat conduction equation for an arbitrary pulse shape. However, the important quantity for calculating local surface temperature evolution is the 3D spatial distribution of the heat flux on the MBs. The near-linearity of the heat conduction equation implies that the local temperature increase ΔT due to a spatially inhomogeneous heat flux distribution can be well approximated by multiplying the 1D result ΔT_{1D} by the ratio of the local heat flux to the reference heat flux, and by an additional factor that takes account of specific geometrical features such as sharp edges, under the condition that the characteristic spatial scale of the profile is not much smaller than the heat diffusion length for a given pulse duration. It is assumed here that this local heat flux ratio is invariant in time, meaning that the ion temperature does not evolve during the ELM.

Two dimensionless quantities are presented in this work. The first is the local heat flux calculated by the 3D ion orbit model normalized to the heat flux to a nominal, axisymmetric surface. The main features of the model are recalled in Section 3. The second is the temperature increase at specific points (flat facets, edges) normalized to the temperature increase predicted by the 1D semi-infinite heat conduction equation, again at a nominal, axisymmetric surface. This latter quantity is valid for any heat pulse shape, making the results useful for predicting the thermal response based on extrapolation from experiments in existing tokamaks, or theoretical modelling of ELM energy deposition patterns. The specific corrections that must be applied at edges are calculated in Section 4. Results will be shown for the proposed ITER design and a number of alternative shaping solutions in Section 5.

The analysis is focused on the inner vertical target (IVT) since twice as much ELM energy is expected to be deposited there than on the outer vertical target [1]. In particular, the long gaps running in the toroidal direction that separate MBs on a given PFU are treated. Results at the magnetically shadowed poloidal leading edges which can receive significant heat flux due to the large Larmor radius of ELM ions are amply discussed in [4]. Plasma parameters corresponding to the 15 MA/5.3 T burning plasma scenario, but also the half-field, half-current scenario typical of the early pre-nuclear phases of ITER operation, will be taken as input to the calculations.

2. Input parameters

For a complete description of the ITER divertor targets along with motivation behind the proposed shaping solution (0.5 mm toroidal bevel) the reader is referred to [7,8]. Here we briefly evoke only those elements needed for our analysis (Fig. 1). In what follows, the term “toroidal gap” (TG) refers to gaps which extend in the toroidal direction separating monoblocks on a given PFU. The toroidal component of the tokamak magnetic field is parallel to a TG. MBs are characterized in this

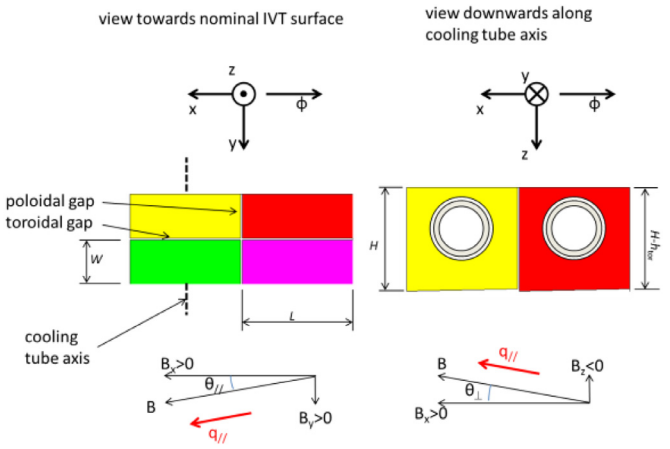

Fig. 1. Local coordinate system and magnetic field orientation at the nominal IVT. The observer is standing in the divertor looking inwards towards the IVT. The magnetic field and the power flow orientations are indicated by arrows. The *x*-coordinate points in the negative toroidal direction. The *y*-coordinate points downward along the cooling tube. The *z*-coordinate is the normal vector of the axisymmetric divertor surface envelope, neglecting shaping. Note the definition of the orientations of the poloidal and toroidal gaps.

study by toroidal length $L = 28$ mm, poloidal width $W = 12$ mm, and radial height $H = 28$ mm. The TG between adjacent MBs on a given PFU is predicted by engineering tolerance build-up to be of width $g_{MB} = 0.4 \pm 0.2$ mm, and the radial step is specified as $m_{rad} = \pm 0.3$ mm.

The magnetic field strength at the IVT is $B = 8$ T in the burning plasma scenario. The angle of incidence between B (projected onto the plane that is perpendicular to the cooling tube axis) and the axisymmetric IVT envelope is $\theta_{\perp} = 3.2°$ at the strike point. In the projection onto the plane that is parallel to front surface of the same axisymmetric IVT envelope, the angle is $\theta_{//} = 3.7°$ The latter angle arises because the magnetic flux surfaces obliquely intersect the IVT.

A 20 mm wide gap between each of the 54 cassettes is imposed by remote handling requirements. As a result, component tilting is required in order to protect the leading edge of each cassette which inevitably arises due to tolerance build-up during the manufacture and installation of these massive cassettes together with assembly tolerances of the vacuum vessel. The exact tilting angle proposed in the current design is approximated here by a rotation of $\Delta\theta = 0.5°$ about the IVT cooling tube axis. The MBs are beveled in the toroidal direction to a depth of $h_{tor} = 0.5$ mm, which hides the poloidal leading edges from inter-ELM heat loads. This leads to an additional angular increment of $\mathrm{atan}(h_{tor}/L) = 1°$ at the top surface of the MBs, such that, accounting for component tilting and MB toroidal bevel, the real total angle between B and the surface is $\alpha \approx \theta_{\perp} + \Delta\theta + h_{tor}/L = 4.7°$ The local surface heat flux is thus about 50% higher than the specified heat loads derived from high heat flux tests. For example, the commonly cited ELM energy density limit of $\varepsilon_{tg} = 0.5$ MJ/m^2 would in reality correspond to $\varepsilon_{surf} = 0.75$ MJ/m^2 locally at each MB. Thus, component tilting and MB beveling reduce the margin against full surface melting.

3. Ion orbit model

The incoming plasma is modelled as a mixture of deuterium and tritium ions having a kinetic distribution of parallel speeds, and a Maxwellian distribution of perpendicular speeds. The electrons are treated under the optical approximation, because their Larmor radii are small enough to be ignored. Electric fields which would arise in the magnetized Debye sheath near the surface

Please cite this article as: J.P. Gunn et al., Ion orbit modelling of ELM heat loads on ITER divertor vertical targets, Nuclear Materials and Energy (2016), http://dx.doi.org/10.1016/j.nme.2016.10.005

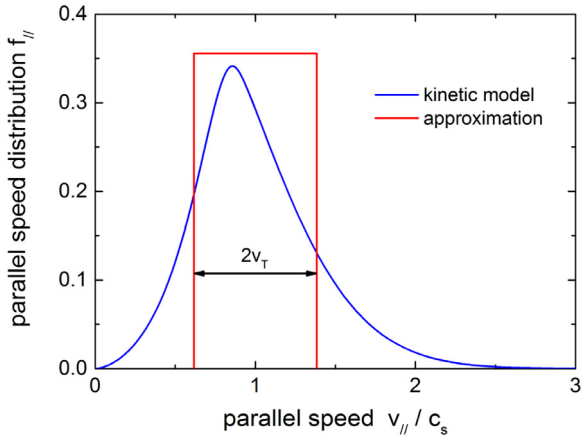

Fig. 2. Parallel speed distribution at sheath edge from a collisionless kinetic model [9] of plasma flow to a surface (blue curve). The red square function is the approximation used by the ion orbit model. It has the same width and mean value as the kinetic distribution. (For interpretation of the references to colour in this figure legend, the reader is referred to the web version of this article.)

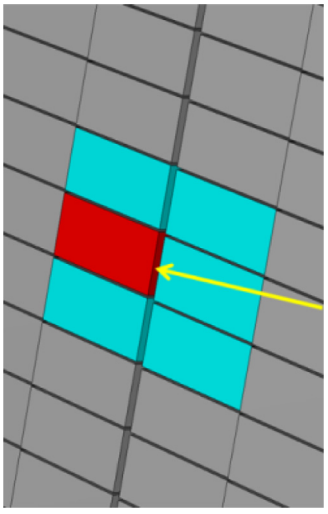

Fig. 3. Simulation environment. In this example, the heat flux to all surfaces of the red MB are to be calculated. Helical ion orbits are followed backwards in time from impact points on the surface. If the trajectory does not intersect any of the 5 neighbouring MBs (coloured cyan), then the ion contributes to the local heat flux (Eq. 4). The arrow indicates the direction of the incident parallel flow. (For interpretation of the references to colour in this figure legend, the reader is referred to the web version of this article.)

are not considered. Only the Larmor gyration of ions due to the Lorentz force is included.

Several Larmor radii away from the surface, the ion velocities are assumed to be described by a collisionless kinetic presheath model [9], which predicts the ion distribution at the entrance of the sheath. All the analysis in this paper assumes plasma with equal concentrations of deuterium and tritium ions. For simplicity, we replace the two species by a single, fictional ion species having mass number $A=2.5$ for the calculation of quantities such as thermal velocity, sound speed, and Larmor radius. We approximate the distribution of parallel speeds $f_{//}(v_{//})$ by a square function having a mean parallel speed $V_{//}$ and thermal width V_T corresponding to the exact kinetic distribution (Fig. 2). The mean parallel speed is in fact the kinetic sound speed

$$V_{//} = c_s = 1.3979\sqrt{\frac{kT_e}{m_i}} \tag{1}$$

and the thermal width from the model is

$$V_T = 0.536\sqrt{\frac{kT_e}{m_i}} \tag{2}$$

with T_e=T_i in the source plasma far upstream. The numerical constants are obtained from the first and second moments of the sheath-edge ion distribution function calculated by the model [9]. The kinetic width of the distribution is smaller than the Maxwellian thermal speed because the ions undergo adiabatic cooling as they accelerate down the presheath to the target. The perpendicular speeds are described by a Maxwellian distribution of temperature T_i

$$f_\perp(v_\perp)\frac{m_i v_\perp}{2\pi kT_i}\exp\left(-\frac{m_i v_\perp^2}{2kT_i}\right). \tag{3}$$

The perpendicular velocity vector is assumed to have a random orientation in the plane perpendicular to $\vec{B}$, described by a phase angle $0 \le \phi \le 2\pi$.

The ion power flux normal to any point on the MB surface is given by the integral

$$q_{surf} = C\int_0^{2\pi}\int_0^{\infty}\int_0^{\infty} R_E(v_{//}, v_\perp, \phi) f_\phi f_\perp f_{//}(\vec{v}\cdot\hat{n}) \times \frac{1}{2}m_i(v_\perp^2 + v_{//}^2)H(v_{//}, v_\perp, \phi)\frac{d\phi}{2\pi}dv_\perp dv_{//}. \tag{4}$$

where f are the distribution functions at the sheath entrance and C is a normalization constant chosen so that the integral yields the parallel power flux $q_{//}$ for the case of an unshadowed surface perpendicular to the magnetic field. Each combination of $v_{//}$, $v_\perp$, and ϕ describes a helical orbit that is followed backwards in time from the moment of impact until the distance between the guiding center and the highest surface feature exceeds the Larmor radius. If an intersection occurs, it will be on one of the five nearest neighbouring MBs (Fig. 3). The mask function $H=1$ if the orbit extends back to the plasma without intersecting any other surface, and $H=0$ if it does (i.e. the orbit is unpopulated because the particle would have struck another surface earlier in time).

Ions and electrons have a probability to reflect from the target [10], carrying away some of their incident energy, resulting in a reduction of the net power flux that is actually absorbed by the surface. The energy and incidence angle of each ion is used to calculate the energy reflection coefficients R_E by the analytical expression Eq. 2.13 on p. 20 of Ref. [10], which are folded into the numerical integral (Eq. 4) of the heat flux. For the electron component of the heat flux, given by the optical approximation, we simply take the value 0.4, which is a reasonable value for reflection from tungsten in the energy range of interest (p. 94 in Ref. [10]).

In order to represent in a heuristic way the filtering effect of the sheath [11], the ion and electron contributions to the power flux are normalized so that they carry respectively 5/7 and 2/7 of the launched parallel power flux. Even though the ion orbit model does not precisely predict the distribution function at the surface, we suppose that the Larmor radius spreading provides an accurate enough stencil of the heat flux spreading. Comparison with PIC simulations of a few representative cases demonstrates the validity of this approximation [12].

4. Monoblock edge heating

The vertical targets are tilted with respect to the magnetic flux surfaces in order to increase power spreading. Magnetic field lines thus intersect the side of each MB that faces upwards towards the X-point. The angle of incidence on these surfaces is in the range $1.5° < \theta_{//} < 7°$ (spanning the full range of magnetic equilibria planned in ITER), which is similar to the angle on the top faces of the MBs, so the power flux to the side of the TG will be of the same order of magnitude as on top of the MB. The power entering

Please cite this article as: J.P. Gunn et al., Ion orbit modelling of ELM heat loads on ITER divertor vertical targets, Nuclear Materials and Energy (2016), http://dx.doi.org/10.1016/j.nme.2016.10.005

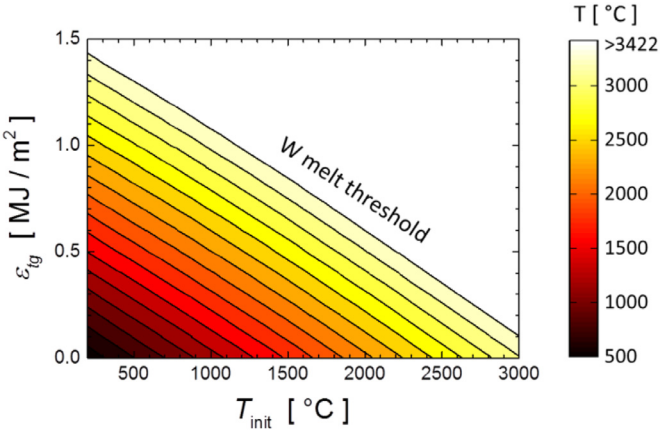

Fig. 4. Peak temperature from solution of the 1D, non-linear, transient heat flux equation. The energy density ε_{tg} to a nominal, axisymmetric divertor target having initial temperature T_{init} is delivered during a triangular pulse having a rise time $\tau_r = 250$ μs and a decay time $\tau_d = 500$ μs. The peak temperature occurs at $t = 460$ μs. The white area corresponds to the onset of melting before the end of the heat pulse.

a TG can be up to 5% ($g_{MB}/(g_{MB}+W) = 0.6\,mm/12.6\,mm$) of the total power impinging on each MB, and since it is deposited on a toroidal edge which is already hot due to loading of the main plasma-facing surface, it is essential to include its contribution to the thermal response. From the point of view of heat conduction, there is a significant difference between an edge that is heated on only one versus both of its facets.

Under the optical approximation only the side of each MB that faces upwards towards the X-point should receive plasma. It is not at all evident that this is realistic because the Larmor gyration of ions is almost purely poloidal. This means that there is a possibility that power can be deposited even on the magnetically shadowed side of a TG if the helicity of the ion orbits is in the correct sense. An observer facing inwards looking at the IVT would see the plasma flowing from right to left, and slightly downwards from the X-point to the target. The bottom, long (toroidal) edges of the MBs, and the left-hand, short (poloidal) edges are magnetically shadowed. Therefore, if the heat flux were purely optical, one would expect to see the top, long edges and the right-hand, short edges overheating (if the edges were not protected by MB shaping). At the IVT, both the upper and lower long edges receive power flux; the top edge receives the electron component of the incident power flux, while the *bottom* edges receive the ions because their Larmor gyration results in an upward vertical motion at the instant of impact. This will be seen in the figures in Section 5.

For the purposes of design work, ITER assumes that the ELM energy is deposited by a heat pulse having a triangular waveform with a decay time $\tau_d = (1–2)\tau_r$ [13]. The less conservative assumption of an asymmetric pulse with $\tau_d = 2\tau_r$ and is assumed in this analysis, since faster decays are not observed in experiments [14]. It is assumed that the rise time of the ELM heat pulse will be $\tau_r = 250$ μs, given by the time of flight of 5 keV pedestal ions from the outboard midplane to the divertor in the burning plasma scenario. For lower values of pedestal temperature, the rise time is increased by the factor $(5000/T_i)^{0.5}$ to reflect the smaller ion thermal speed.

Fig. 4 shows the surface temperature on a semi-infinite domain after exposure to an ELM heat pulse. Convex features such as edges and corners heat up more than flat surfaces. Simple linear analysis illustrates the problem well. Consider the sharp edge of a body delimited by the space $x \geq 0$ and $z \leq 0$. Uniform heat fluxes q_{side} and q_{top} are applied normal to the side and top surfaces, respectively, for a duration of $\Delta t_{ELM} = 250$ μs. In the linear problem with constant thermal properties, the temperature throughout the body is given by the linear superposition of the solutions of two simpler problems. For the case of heat flux applied only to the side surface, the solution is identical to that of the 1D, semi-infinite problem

$$T_{side}(x,t) = \frac{\sqrt{\alpha_h} q_{side}}{\kappa}\left(2\sqrt{\frac{t}{\pi}}\exp\left(-\frac{x^2}{4\alpha_h t}\right) - \frac{x}{\sqrt{\alpha_h}} erfc\frac{x}{2\sqrt{\alpha_h t}}\right), \tag{5}$$

and for the case of heat flux applied only to the top surface, the solution is

$$T_{top}(z,t) = \frac{\sqrt{\alpha_h} q_{top}}{\kappa}\left(2\sqrt{\frac{t}{\pi}}\exp\left(-\frac{z^2}{4\alpha_h t}\right) + \frac{z}{\sqrt{\alpha_h}} erfc\frac{-z}{2\sqrt{\alpha_h t}}\right). \tag{6}$$

where α_h is the thermal diffusivity and κ is the thermal conductivity. The 2D solution is

$$T(x,z,t) = T_{top}(z,t) + T_{side}(x,t). \tag{7}$$

The temperature at the sharp edge is exactly equal to the sum of the surface temperatures on the individual facets at positions sufficiently far from the edge where the 1D solution is recovered.

An approximate procedure has been developed to calculate the temperature increase at an edge using power flux profiles whose spatial variations cannot be considered to be uniform. The local heat flux is averaged over one heat diffusion length along the surface around the point of interest. The heat diffusion length is the assumed to be equal to the characteristic depth of the heated layer on either surface far from the edge

$$\Delta s = \sqrt{2\alpha_h \Delta t_{ELM}}. \tag{8}$$

Taking high temperature values of the thermal properties of tungsten, $c_p = 180$ J/kg/K and $\kappa = 100$ W/m/K, and taking the characteristic time to be when the surface temperature peaks, $\Delta t_{ELM} = 460$ μs, the depth of the heated region is about $\Delta s \sim 160$ μm for the triangular pulse.

A specified ELM heat flux q_{tg} to a nominal target produces a certain peak temperature increase (Fig. 4), referred to as ΔT_{1D}. The local peak temperature at a MB edge can be expressed in terms of ΔT_{1D}

$$\frac{\Delta T}{\Delta T_{1D}} = f_{geo}\frac{\int_{S_{edge}-\Delta s}^{S_{edge}+\Delta s} q_{surf} ds}{2\Delta s\, q_{tg}} \tag{9}$$

where the heat flux profile is integrated along a surface coordinate s running over the edge centered at s_{edge}, and f_{geo} is a numerical factor related to the edge geometry. At a sharp edge with temperature-independent material properties, the factor is exactly $f_{geo} = 2$. For non-linear material properties, the factor is $f_{geo} = 2.1$. The non-linearity is weak because the increase of heat capacity with temperature nearly compensates the decrease of heat conductivity, making the thermal effusivity nearly independent of temperature. The geometrical factor has been calculated by the finite element software package ANSYS for a range of edge angles and for a range of radius of curvature in the case of filleted (rounded) edges (Fig. 5). To obtain this factor, heat flux was applied uniformly over an edge having an initial temperature $T_{init} = 100$ °C. The peak temperature increase was divided by that obtained far enough from the edge that the heat flow into the bulk could be considered to be one-dimensional. This simple procedure avoids the need to make a 2D finite element calculation for each case. Comparison with a full 2D heat flow calculation using heat flux profiles given by the ion orbit model as input shows that the accuracy of the predicted edge temperature increase is of the order of 1%, which is acceptable for scoping studies such as this.

Please cite this article as: J.P. Gunn et al., Ion orbit modelling of ELM heat loads on ITER divertor vertical targets, Nuclear Materials and Energy (2016), http://dx.doi.org/10.1016/j.nme.2016.10.005

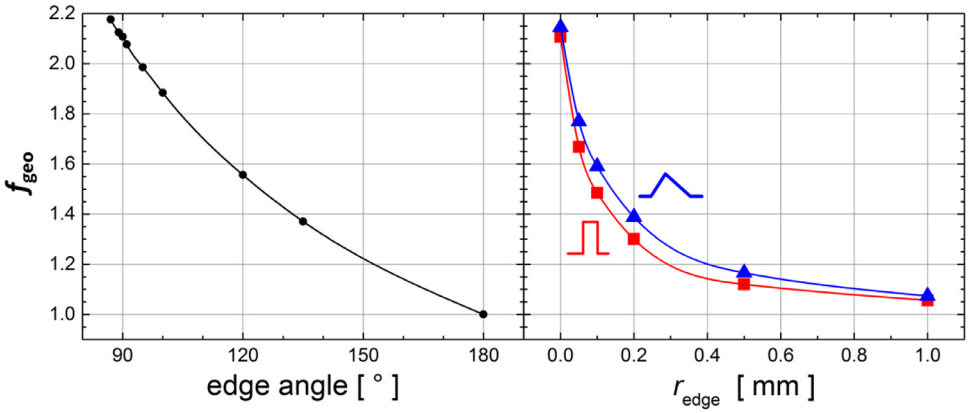

Fig. 5. Enhancement of peak temperature at an edge due to a fast heat pulse. At left the factor is calculated at a sharp edge as a function of the angle. Sharp right angle edges are 90°; the limit of a flat surface is 180° At right the factor is calculated at a filleted (rounded) edge as a function of the radius of curvature for square and triangular heat pulses (square and triangular symbols, respectively).

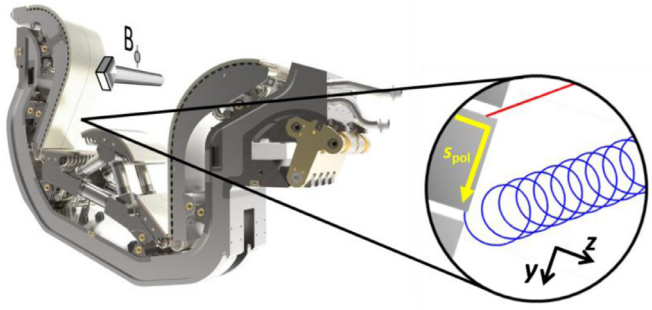

Fig. 6. An ITER divertor cassette showing orientation of toroidal magnetic field. The inset is a zoom on an IVT MB showing a typical ion orbit projected onto the poloidal plane, and the definitions of coordinates that will appear in the following figures. The *s* coordinate runs poloidally over the surface of the MB from the magnetically wetted edge to the shadowed edge, *y* points downward along the cooling tube axis, and *z* is perpendicular to the top MB surface.

5. Results

Power loads were calculated by the ion orbit model for plasma conditions corresponding to the 15 MA/5.3 T burning plasma scenario with $T_i = 5000$ eV, and for the half current / half field (7.5 MA/2.65 T) scenario with $T_i = 2500$ eV Ion mass $A = 2.5$ was assumed in both cases for simplicity. For the latter scenario, representative of early, pre-nuclear phases of ITER operation, the working gas will likely be helium since it has a lower power threshold for the transition from L-mode to H-mode than hydrogen does. Helium ions coming to the divertor from the hot pedestal will be doubly ionized, so they will have the same charge-to-mass ratio, and thus the same Larmor radius, as deuterium. The calculation results are not very sensitive to the ion species, so this simplification is justifiable.

In the following, power load profiles are shown for MBs that are radially aligned with their neighbours on a given PFU, but with the widest tolerable gaps (presently specified as 0.6 mm). The definition of the coordinate system used in this analysis can be seen on Fig. 6. Ion orbits terminating on the point that receives the highest heat flux will be illustrated. The edge temperature enhancement with respect to an ideal, axisymmetric divertor target is calculated for the full range of radial misalignments and TG widths. At the top MB surface far from the gaps, the enhancement is already 1.5 with respect to the nominal value due to toroidal bevel plus component tilting.

5.1. Sharp edges

In contrast to PGs which receive plasma only on the side that faces upstream towards the SOL, TGs can be irradiated on the magnetically shadowed side if the ion Larmor gyration has the correct helicity. At the IVT, the direction of rotation about the ion guiding center is such that ions strike the lower, magnetically shadowed MB edges, whereas the opposite occurs at the OVT. The ELM heat flux across a poloidal section of IVT MBs, far from the poloidal leading edge where the toroidal variations are negligible, is shown in Fig. 7 for the full field, burning plasma scenario. The heat flux at the top surface is about 50% higher than the nominal value because of the increased *B*-field angle of incidence due to $\Delta\theta = 0.5°$ target tilting plus 1° associated with the $h_{tor} = 0.5$ mm toroidal bevel. The peak of heat flux beyond $s_{pol} = 12$ mm is due to ions gyrating into the magnetically shadowed side of the TG. The scale length of the profile inside the gap is about 400 µm, which is larger than the heat diffusion length of 160 µm, making the simple thermal analysis applicable. The heat flux before $s_{pol} = 0$ mm is carried by the electrons onto the magnetically wetted side of the TG.

Also in Fig. 7a poloidal section of the MBs is shown. The two cycloidal curves bracket the ion orbits that can access the top of the TG. The red orbit is limited by grazing impact on the top surface of the MB, while the blue orbit is limited by the corner of the downstream MB. The angle between the orbits at the impact point gives a qualitative indication of the intensity of the heat flux striking the MB at that position.

The enhancement of the temperature peak at the lower TG edge with respect to the prediction at a nominal target surface during an ELM burst is shown in Fig. 8 for the range of assembly tolerances presently specified in the ITER IVT design. Both full and half field scenarios are shown. There is not much difference between them; for well-aligned MBs, the edge temperature is about three times higher than the nominal temperature for both scenarios. The peak temperature is nearly invariant with increasing TG width; this is because the allowed orbits arrive at nearly grazing angles of incidence with respect to the top surface, and their Larmor radii are much larger than the gap width. There is a stronger variation as a function of the radial step; MBs that are deeply recessed receive less power flux at the top of the TG because the ion orbits are creamed off by the downstream MB.

It is not visible on Fig. 8, but what does vary with gap width is the depth of the deposition profile inside the gap. Wider gaps allow ELM ions to penetrate deeper into the TG. At deeper positions, the simple thermal analysis that is applicable directly at an edge

Please cite this article as: J.P. Gunn et al., Ion orbit modelling of ELM heat loads on ITER divertor vertical targets, Nuclear Materials and Energy (2016), http://dx.doi.org/10.1016/j.nme.2016.10.005

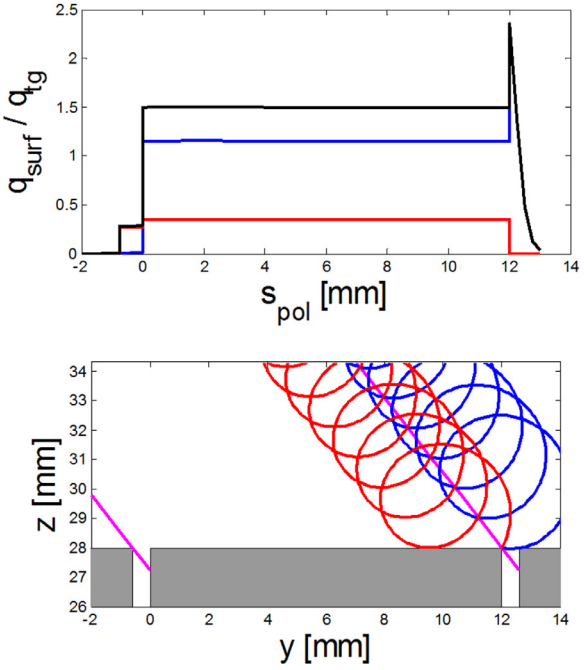

Fig. 7. Heat flux and ion orbits at MBs with sharp edges assuming no radial misalignment, but with the widest acceptable TG width. Upper panel: surface heat flux normalized to the heat flux to a nominal target. The red curve is the electron component which assumed to obey the optical approximation, the blue curve is the ion component calculated by the ion orbit model, and the black curve is the sum of the two. Lower panel: poloidal cross section showing the two extremes of orbits whose gyrophase allows the ions to reach the top of the TG. Both orbits have parallel speed equal to the sound speed, and perpendicular speed equal to the thermal speed. The straight lines indicate the magnetic flux surfaces. These curves correspond to the full field, burning plasma scenario with $T_i = 5$ keV and $B = 8$ T at the IVT strike point.

is less reliable, and full 2D thermal calculations are required. This has been done for gap widths of 0.2 and 0.6 mm, assuming a nominal incident energy density of $\varepsilon_{tg} = 0.5\ \mathrm{MJ/m^2}$. The depth of the zone that exceeds the melting temperature of tungsten (3422 °C) is 39 μm for the narrowest gap, and 62 μm for the widest gap. These calculations do not treat liquid tungsten; the thermal properties for temperatures higher than the melt temperature are simply assumed to be equal to those at the melt temperature. Calculations with more sophisticated codes such as MEMOS would be required to go further, but it is reasonable to conclude that wider gaps potentially result in broader melt layers inside TGs.

The data in Fig. 8 apply to any surface energy density and pulse shape, once the nominal 1D thermal response to that pulse is known. For example, the nominal temperature increase corresponding to the full field scenario with $\Delta t_{ELM} = 250$ μs can be read from Fig. 4, and the temperature multiplied by the number from the left panel of Fig. 8 to obtain the temperature increase at the lower toroidal MB edge. Strictly speaking, the temperature enhancement would have to be recalculated for pulse shapes having a different rise time, because the heat diffusion length will vary. This means that the integral of the heat flux profile over the edge would change slightly. However, since the characteristic scale length of the profiles inside the TG are typically larger than the heat diffusion length, and since that length varies weakly with the rise time, the correction would be negligible. As long as the rise time is not, say, an order of magnitude different that the value assumed in this analysis, the results of Figure 8 can be used for scoping studies.

The maximum nominal surface energy density is generally accepted to be $\varepsilon_{tg} = 0.5\ \mathrm{MJ/m^2}$, which leads to a temperature increase of $\Delta T_{1D} = 1100$ °C. The edge of a well-aligned MB in the burning plasma scenario would heat up 3.5 times higher than that, pushing the edge well into melting even if the MB were initially cold. If edge melting avoidance is taken as a design criterion for an ELM mitigation system, for example, the maximum nominal surface energy density would have to be reduced to $\varepsilon_{tg} = 0.14\ \mathrm{MJ/m^2}$.

5.2. Chamfered edges

A natural proposal to avoid melting at sharp TG edges is to remove the zone that melts by appropriate poloidal profiling. Calculations have been made for MBs with a 1 mm chamfer applied to their long edges (Fig. 9). This results in an edge having an angle of 135°, which means less intense temperature peaking. From Fig. 5 the geometrical peaking factor is about $f_{geo} = 1.4$ instead of 2.1. However, chamfering opens up the TG, allowing more ions to access the surface. Instead of arriving at grazing angles, ions can now spiral down into the gap and back up onto the edge. In fact, the gap is so wide that ions are no longer creamed off by the adjacent MB. The flux to the edge is determined only by the Larmor radius, independent of misalignments. For that reason the type of graph shown in Fig. 8 for the sharp edge is not shown here; the temperature enhancement is about 2.9 for full and half field scenarios, independent of misalignment. The net result is no significant improvement with respect to sharp-edged MBs. Melting is not avoided, it just occurs elsewhere. A further problem with this shaping solution is at the upstream TG edge. That edge is now more exposed to inter-ELM heat loads, which will lead to higher

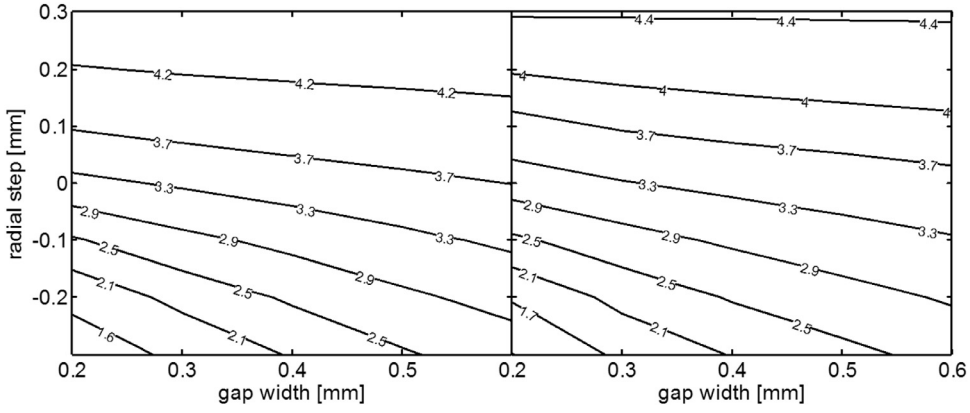

Fig. 8. Peak edge temperature enhancement with respect to an ELM pulse to a nominal target for the full field scenario with $T_i = 5$ keV (left panel) and half field scenario with $T_i = 2.5$ keV (right panel) for the range of assembly tolerances presently specified in the reference ITER IVT design.

Please cite this article as: J.P. Gunn et al., Ion orbit modelling of ELM heat loads on ITER divertor vertical targets, Nuclear Materials and Energy (2016), http://dx.doi.org/10.1016/j.nme.2016.10.005

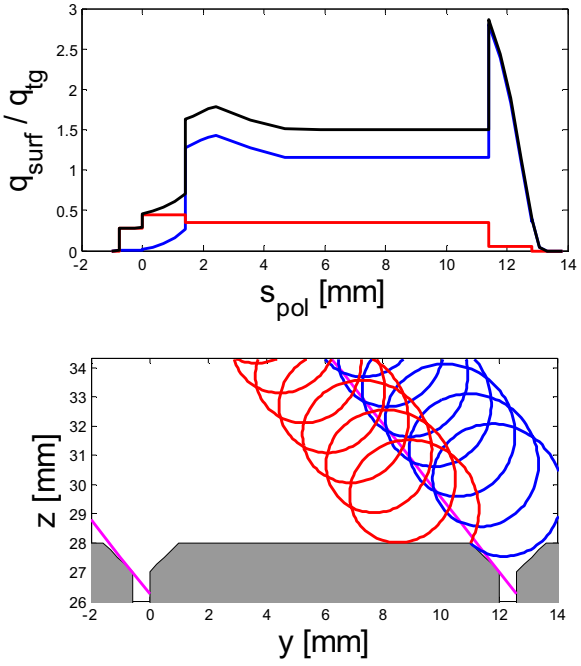

Fig. 9. Heat flux and ion orbits at a 1 mm chamfered edge. Same indications as Fig. 7.

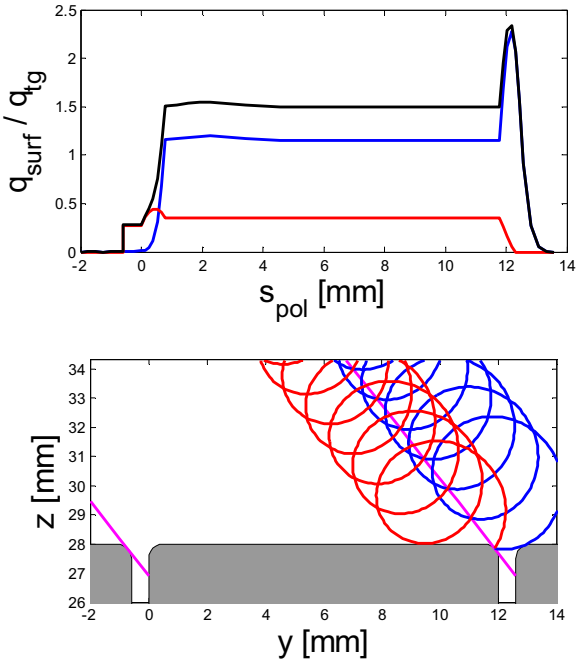

Fig. 10. Heat flux and ion orbits at a 0.5 mm filleted (rounded) edge. Same indications as Fig. 7.

steady state temperatures, and reduce the margin against tungsten recrystallization.

5.3. Filleted edges

Chamfered edges are still sharp, and it seems that ion flux tends to focus on regions where there is a sharp boundary between two facets having different orientations. From Fig. 5 it is seen that the geometrical peaking factor at filleted (rounded) edges falls quickly to unity once the radius of curvature of the fillet exceeds the heat diffusion length. Therefore, the calculations were repeated for a smooth edge having a radius of curvature of 0.5 mm (Fig. 10). The heat flux is maximum at the center of the arc, but is similar to the magnitude predicted for sharp edges. The resulting heating is essentially 1D, and so less severe. The edge temperature enhancement factor is identical for full and half field scenarios; it varies little with gap width, and increases from 1.9 for the most recessed MBs to 2.9 for the most protruding ones.

5.4. Poloidal bevel

The shaping options presented above all suffer from the same phenomenon. Ions gyrate into the TG and are focused there. Rather than trying to modify the edges, a different solution consists of profiling the entire top surface of the MB to hide the edge from this Larmor radius flux. In addition to the 0.5 mm toroidal bevel that protects the poloidal leading edge from inter-ELM heat loads, an additional poloidal bevel could be superimposed such the edge is shadowed by the downstream MB. It is not trivial to choose values for the two bevel depths because of the requirement to protect poloidal leading edges. For example, if a poloidal bevel of $h_{pol} = 0.2$ mm were applied upon the existing $h_{tor} = 0.5$ mm toroidal bevel, given the tolerance of $m_{rad} = 0.3$ mm on the radial misalignment between PFUs, it is possible that part of the leading edges would be directly exposed to the parallel flux. To avoid that, it is necessary to make the toroidal bevel deeper, which obviously has the disadvantage of further increasing the local magnetic field

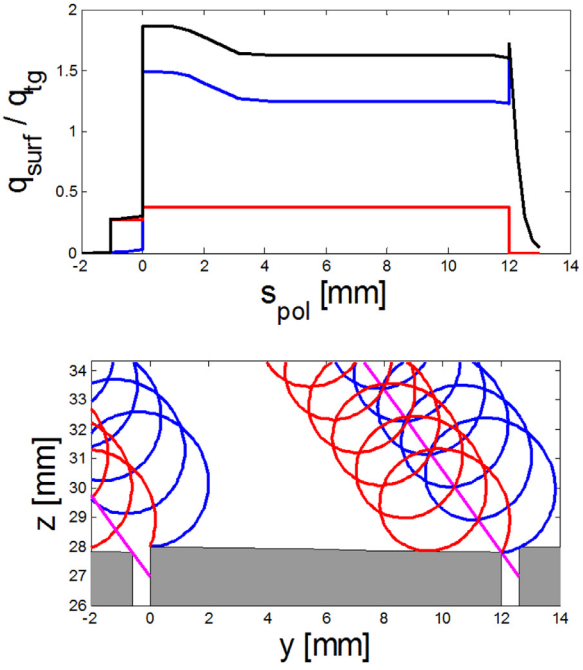

Figure 11. Heat flux and ion orbits on a MB with a toroidal bevel of $h_{tor} = 0.7$ mm and a poloidal bevel of $h_{pol} = 0.2$ mm. Same indications as Fig. 7.

angle and thus reducing the MB power handling capacity and margin against critical heat flux. Calculations have nonetheless been made with a toroidal bevel of $h_{tor} = 0.7$ mm combined with an $h_{pol} = 0.2$ mm poloidal bevel (Fig. 11).

A number of curious things happen. The heat flux to the magnetically shadowed edge does indeed decrease because few ions can reach it. This is visible in that the angle between the two orbits is clearly smaller than in the earlier cases. In fact, the situation is nearly identical to a sharp edge of a MB that is recessed by 0.2 mm with respect to its neighbours (Fig. 7). Power balance

Please cite this article as: J.P. Gunn et al., Ion orbit modelling of ELM heat loads on ITER divertor vertical targets, Nuclear Materials and Energy (2016), http://dx.doi.org/10.1016/j.nme.2016.10.005

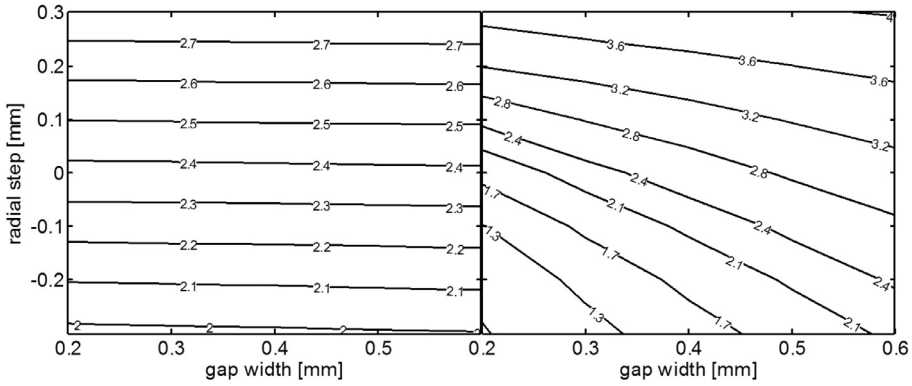

Fig. 12. Peak edge temperature enhancement with respect to an ELM pulse to a nominal target for the full field scenario with $T_i = 5$ keV for the range of assembly tolerances presently specified in the reference ITER IVT design. The left panel corresponds to the upstream MB edge (left hand edge in lower panel of Fig. 11), while the right panel corresponds to the downstream edge.

must be preserved, so where does the lost power go? It is now absorbed by the upstream edge of the adjacent MB. Since that edge is now protruding, it is also more exposed to the electron component of the heat flux, and inter-ELM heat loads. The net result is that the two long edges share the power flowing into the gap about equally; both edges have a temperature enhancement factor of about 2.4 (Fig. 12). At the upstream edge this factor does not vary with gap width, but increases from 2.0 to 2.8 with increasing radial misalignment. At the downstream gap, the benefit of poloidal beveling is lost when the MB starts to protrude ahead of its neighbours. The results are identical for full and half field scenarios, so only the former is shown here.

6. Discussion

A new scaling for parallel energy density $\varepsilon_{//}$ released during uncontrolled Type I ELMs has recently been proposed [3]. The essence of those findings is that $\varepsilon_{//}$ (that is, the peak parallel power flux integrated over the duration of the ELM event) is proportional to the pedestal pressure, and that the poloidal width of the ELM footprint increases with ELM size. For the half current, half field scenario ($I_p = 7.5$ MA, $B = 2.65$ T) representative of the pre-nuclear experimental campaigns, the prediction for the surface energy density obtained by projecting $\varepsilon_{//}$ onto the ideal, axisymmetric ITER vertical target is $0.125 < \varepsilon_{tg} < 0.375\,\mathrm{MJ/m^2}$, while for the burning plasma scenario ($I_p = 15$ MA, $B = 5.6$ T), it is $0.5 < \varepsilon_{tg} < 1.5\,\mathrm{MJ/m^2}$.

Even though our analysis concerns the IVT, the results presented here will be cast in terms of this new scaling which corresponds to the outer target, because a similar scaling for the inner target is not yet available. For the pre-nuclear scenario, assuming an ELM rise time of $\Delta t_{ELM} = 350$ μs and $T_i = 2.5$ keV, the nominal surface temperature increase is calculated by the 1D heat equation to be in the range $200 < \Delta T_{1D} < 700$ °C. Multiplying the highest expected temperature increase by the calculated edge enhancement factors, the temperature increase at the magnetically shadowed toroidal MB edge has been calculated for the present ITER design with sharp edges, and the alternative design that incorporates an additional poloidal bevel (Fig. 13). In the case of sharp edges, the temperature increase is quite high. Whether this is a problem depends on the relative alignment of the MBs, but also on their mean temperature, which is set by the total average power flow to the divertor integrating both inter-ELM and ELM heat loads. From [4], the mean MB temperature will probably not exceed 800 °C in this regime. The highest surface energy densities could cause edge melting if they strike radially misaligned MBs. Even though the tolerance on the radial step between MBs on a given PFU is specified as ±0.3 mm, it is expected that the obtained tolerance will not exceed ±0.1 mm [15]. The risk of sharp edge melting in the pre-nuclear phase can perhaps be described as marginal. A gain of several 100 °C could be obtained by implementing a poloidal bevel, but this has to be balanced against the reduced heat handling capacity of MBs with a necessarily steeper toroidal bevel.

In the burning plasma scenario at full current and full field, the predicted surface energy densities correspond to peak temperatures $1000 < \Delta T_{1D} < 3200$ °C. Mean MB temperatures could be as

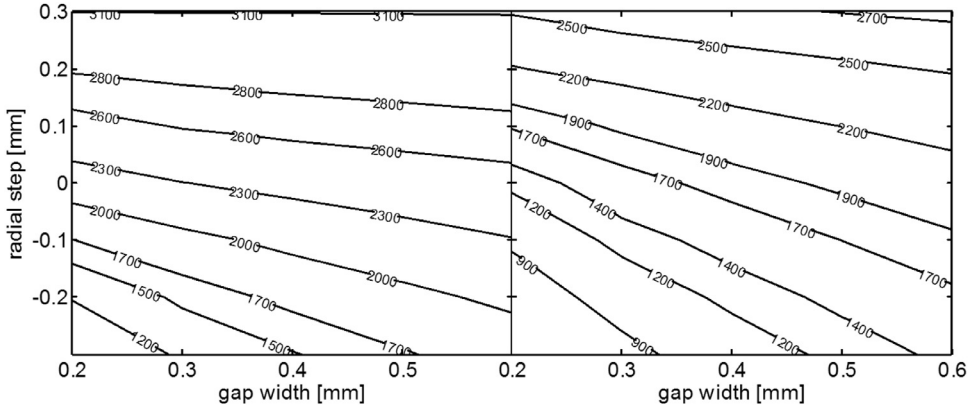

Fig. 13. Peak edge temperature during ELMs for the pre-nuclear, half field scenario with $T_i = 2.5$ keV for the range of assembly tolerances presently specified in the reference ITER IVT design. The worst case surface energy density predicted by a recent empirical scaling [3] $\varepsilon_{tg} < 0.375\,\mathrm{MJ/m^2}$ is taken as input. Left panel: MBs with sharp edges; right panel; MBs with a poloidal bevel of $h_{pol} = 0.2$ mm.

Please cite this article as: J.P. Gunn et al., Ion orbit modelling of ELM heat loads on ITER divertor vertical targets, Nuclear Materials and Energy (2016), http://dx.doi.org/10.1016/j.nme.2016.10.005

high as 1000–1500 °C, depending on the radiated power distribution, and the balance of SOL power between the inner and outer targets [4]. It is clear that even ELMs producing energy densities at the lower boundary of the scaling will melt the toroidal edges, whichever shaping solution is considered.

The modelling tools used in this work are based on significant simplifications that allow large numbers of cases to be studied in the framework of scoping studies. It is therefore important to compare with more rigorous calculations, as they become available. Two-dimensional particle-in-cell simulations including self-consistent electric fields were performed to model MBs with sharp edges [12] for a few specific cases. The results compare surprisingly well with the simple ion orbit model. Recently, simulations have been made of the poloidal gaps of flat-topped MBs with no misalignments, but with sharp, chamfered, and filleted leading edges. The heat flux was calculated by a 2D PIC code, and the thermal model includes a treatment of the liquid phase of tungsten. The results are not directly comparable with this work which treats toroidal edges, but the authors did conclude that although filleted edges perform the best, they still melt [16].

7. Conclusions

ELM heating at the magnetically shadowed toroidal edges of IVT MBs was identified as being severe in Ref. [4]. The heating occurs due to the Larmor gyration of hot ions that focus heat flux at the top of the toroidal gaps. Alternative shaping solutions including chamfering, filleting, and an additional poloidal bevel were evaluated in this paper. The results are broadly the same. Removing the sharp edge just results in the overheated zones migrating to other locations on the MB. While slight gains are obtained by filleting and poloidal beveling, the result must be balanced against the increased cost and manufacturing complexity of such solutions, as well as other detrimental effects such as increased exposure of the edges to inter-ELM heat loads due to the wider gap openings.

Without ELM mitigation, there is a marginal risk of edge melting due to uncontrolled ELMs in the pre-nuclear phase of ITER operation, and an absolute certainty of it in the burning nuclear phase. To avoid edge melting altogether, the surface energy density would have to limited to less than 0.15 MJ/m^2.

Disclaimer

The views and opinions expressed herein do not necessarily reflect those of the ITER Organization.

Funding

This work was supported within the framework of the SSA 29 – ITER/IA/13/ 4,300,000,827 “Full-W divertor: assessment of target monoblock shaping for the safe operation of the ITER machine”.

References

[1] A. Loarte, et al., Nucl. Fusion 47 (2007) S203.
[2] R.A. Pitts, J. Nucl. Mater. 415 (2011) S957.
[3] T. Eich, et al., these proceedings.
[4] J.P. Gunn, S. Carpentier-Chouchana, Y. Corre, R. Dejarnac, F. Escourbiac, M. Firdaouss, T. Hirai, M. Kočan, M. Komm, A. Kukushkin, P. Languille, M. Missirlian, S. Panayotis, R.A. Pitts, W. Zhao, G. Zhong, Surface heat loads on the ITER divertor vertical targets, Nucl. Fusion (2016).
[5] G. Pintsuk, et al., Fus. Eng. Des. 82 (2007) 1720.
[6] J.H. Yu, G. De Temmerman, R.P. Doerner, R.A. Pitts, M.A. van den Berg, Nucl. Fusion 55 (2015) 093027.
[7] T. Hirai, F. Escourbiac, S. Carpentier-Chouchana, et al., Fus. Eng. Des. 88 (2013) 1798.
[8] S. Carpentier-Chouchana, T. Hirai, F. Escourbiac, et al., Phys. Scr. T159 (2014) 014002.
[9] K.-S. Chung, I.H. Hutchinson, Phys. Rev. A 38 (1988) 4721.
[10] R.A. Langley, J. Bohdansky, W. Eckstein, P. Mioduszewski, J. Roth, E. Taglauer, E.W. Thomas, H. Verbeek, K.L. Wilson, in: Data Compendium for Plasma–Surface Interactions, Nucl. Fusion, Special Issue 1984, IAEA, Vienna, 1984, pp. 12–27.
[11] P.C. Stangeby, Phys. Fluids 27 (1984) 682.
[12] M. Komm, et al., submitted to Nucl. Fusion.
[13] A. Loarte, et al., in: 2010 Proc. 23rd Int. Conf. on Fusion Energy, Daejeon, South Korea, 2010 [ITR/1–4].
[14] T. Eich, H. Thomsen, W. Fundamenski, G. Arnoux, S. Brezinsek, S. Devaux, A. Herrmann, S. Jachmich, J. Rapp, JET-EFDA contributors, J. Nucl. Mater. 415 (2011) S856.
[15] F. Escourbiac, ITER Organization, private communication (2016).
[16] Y. Huang, J. Sun, W. Hu, C. Sang, D Wang, Fus. Eng. Des. 102 (2016) 28.